FIELD OBSERVATIONS OF TURBULENCE OVER A GRAVEL BEACH

Zhi-Cheng Huang[1,2], Wu-Ting Tsai[3], Philip L.-F. Liu[4]

Field measurements of waves, current, and turbulence over a gravel beach are presented using dual ADVO techniques. Turbulence was decomposed using a filtering technique; the quality of the estimated turbulence was examined using ogive curve testing on turbulent shear stress (TSS) to remove wave biased containment. The turbulent dissipation rate was estimated using inertial subrange techniques. The ratio of the TSS to TKE is found to smaller than that in a current-alone flow, suggesting that transport of TKE into the bottom boundary layer (BBL) might be important. The turbulent dissipation rate is found to exceed the shear production, which also indicates the transport of TKE into the BBL might be important. After examining the most terms in the TKE budget as possible, we found that the observed vertical turbulent transport is comparable to the shear production, and contributes to part of gaining TKE in the BBL.

Keywords: gravel beach; turbulence; boundary layer; coastal zone

1. INTRODUCTION

Predictions of nature coastal dynamics, sediment transport, and contaminant spreading require understandings of turbulence in the surf and swash zones. The water column shoreward the continental shelf in a nature nearshore environment is composed of three regions: a surface boundary layer (SBL), a central region, and a bottom boundary layer (BBL) (Grant and Madsen, 1986). It has been recognized that turbulence in the oceanic water column is mainly generated from wave breaking in the upper surface boundary layer, and from the bottom drag in the bottom boundary layer. Overlapping of the two layers complicates the turbulence mixing in shallow surf zones.

The vertical shear of mean flow induced by the bottom drag produces turbulence in a general wall BBL. Assuming a constant stress layer over the viscous sublayer and the turbulent production is balanced by the dissipation, a typical BBL scaling exists:

$$\varepsilon = \frac{u_*^3}{\kappa z}, \tag{1}$$

where ε is the turbulent dissipation rate, u_* is the friction velocity, κ is the von Kármán's constant, and z is the height above the bed. It has been questioned whether such a scaling law exists in nature nearshore BBL. Many observational studies have shown that the scaling law exists under a unidirectional current flow conditions without the effects of waves, such as the tidal current in a continental shelf (Gross and Nowell, 1983; Sanford and Lien, 1999), and the unidirectional water flow over coral reefs (Reidenbach et al., 2006). Perlin et al. (2005) modified the scaling law to fit the low velocity gradient region further above the BBL for tidal current and outflow plume. Under the effects of whitecapping waves, wind, and tidal forcing in estuarine embayment (about 2.5 m deep), Jones and Monismith (2008) found that the turbulent dissipation rate ε was approximately equal to or less than that predicted by the BBL scaling. However, Feddersen et al. (2007), Grasso et al. (2012), and Feddersen (2012) showed that ε does not follow the BBL scaling under shallow water (about 3.2 m deep) under the effects of whitecapping waves.

When the water is shallow enough, wave orbital velocities can extend to the seabed and creates the wave bottom boundary layer (WBBL). Grant and Madsen (1979) theoretically extended the concept of current boundary layer to include the presence of wave-orbital velocities. Field observations for the WBBL have been carried out by Conley and Inman (1992), Trowbridge and Agrawal (1995), Foster et al. (2000), Foster et al. (2006), Smyth and Hay (2003). However, most of the field studies focused on the boundary layer process over sandy bottoms. Turbulence over rough bottom, such as coral and algal reefs in the shallow tidal zone in the presence of currents and waves, however, has rarely been studied.

Studies on hydrodynamics and turbulence over naturally rough seabed conditions. However, turbulent properties in natural coal and algal reefs have only been revealed by several studies in recent years. Reidenbach et al. (2006) measured boundary layer turbulence with ADVs for unidirectional flows over the fringing coral reefs in the Red Sea. Because most of the coral reefs and algal reefs are

[1] Graduate Institution of Hydrological and Oceanic Science, National Central University, Taoyuan 320, Taiwan.
[2] International Wave Dynamics Research Center, National Cheng-Kung University, Tainan 701, Taiwan.
[3] Department of Engineering Science and Ocean Engineering, National Taiwan University, Taipei 106, Taiwan
[4] School of Civil and Environmental Engineering, Cornell University, Ithaca, New York 14853, USA.

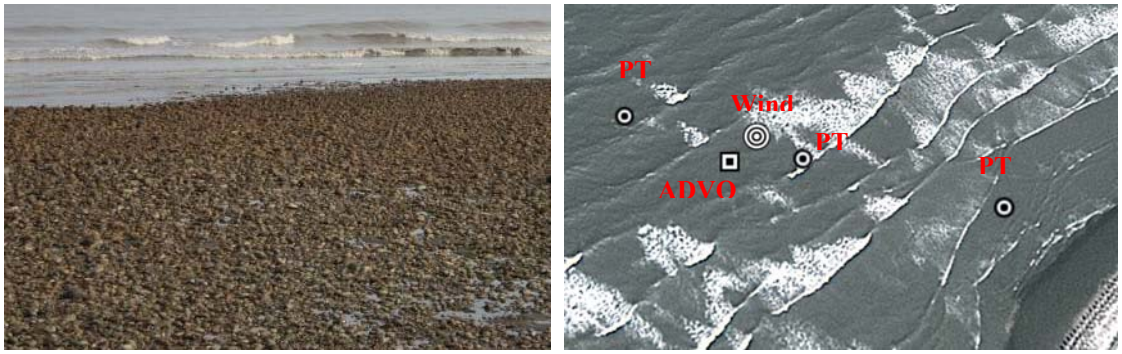

Figure 1. Picture of the study site, the gravel beach off the north-west coast of Taiwan.

exposed in wave-induced oscillatory flow environments, it is not clear how waves affect the turbulent properties in wave dominant coastal environments. Huang et al. (2012) applied wave gauge and ADV techniques to observe the wave and turbulent dissipation rates over the coral reefs surrounding LEI, GBR, Australia. The observed turbulent dissipation rate is about a factor of 1.5 to 2.4 of the surface wave energy dissipation rate when the turbulent dissipation rate is scaled using depth-integrated approach and a bottom boundary layer scaling (Eq. (1)). This indicates a highly efficient conversion of wave motion into turbulence mixing in the lagoon. Thompson et al. (2012) experimentally examined the wave friction factor on a gravel bed. Few have examined the turbulence over coarse seabed such as those found on gravel beaches in field. Possible interaction between the energetic wave breaking induced turbulence and the rough seabed induced turbulence may further complicate the mixing in the shallow water column. Field observations of turbulence in the surf zone and the BBL process on a rough gravel beach are largely unexplored.

Here we present field measurements of turbulence over a gravel beach using ADV techniques. Wave energy flux and wave dissipation rate were measured by pressure sensors. Turbulence properties in the wave-current BBL over the WBBL on a rough gravel seabed site are studied.

2. EXPERIMENTS

2.1 Experimental facilities and setup

The field experiment was conducted over a gravel beach (Figure 1) located off the north-west coast of Taiwan (Shinwu Village, Taoyuan county; 24.967N, 121.007E) during June 28 – July 11, 2013. The gravel beach is mainly covered by sand, pebbles, and cobbles, which produce rough seafloor surface. The bottom topography and the seabed features over the gravel beach were determined using a portable scanning light detection and ranging (LIDAR) system. The along-track spatial resolution of the LIDAR is about 4 - 5 cm. The bottom slope of this beach is about 1/60. Preliminary analysis of the topography shows that the standard deviation values of bottom roughness on the beach are about 4 - 7 cm.

A suite of instruments was deployed along a line in cross-shore direction to make measurements of wind, waves, currents, and turbulence over the beach. Three pressure and temperature sensors were deployed in the cross-shore direction to measure the wave height and energy flux at 4Hz. Two 5-MHz SonTek acoustic Doppler velocimetry-Ocean (ADVO), were side-looking oriented and mounted as a vertical array on a stainless-steel frame. The two ADVOs were set to continuously sample the 3-D flow velocities at 20 Hz. The sampling points of the ADVOs were at 0.26 m (ADVO1) and 0.68 m (ADVO2) above the seafloor. A stainless steel tower was fixed on the seafloor near the velocimetry array. An ultrasonic anemometer was installed on the tower to measure the wind data at 20 Hz.

2.2 Data analysis

The quality of the measured velocity data were determined based on the backscattered signal amplitude and the correlation coefficients following the guideline of Elgar et al. (2005). Velocity series with signal amplitude less than 100 or correlation threshold < 0.7 were indentified as outliers. If any velocity component was indentified as a spike noise, all three components of velocities were identified as a spike noise. Despiking of the outliers was then proceeded using 3-D phase space method and interpolated using the method proposed by Mori et al. (2007). Despiking and interpolation of the outliers was then proceeded using the 3-D phase space method. Despiked velocities were then

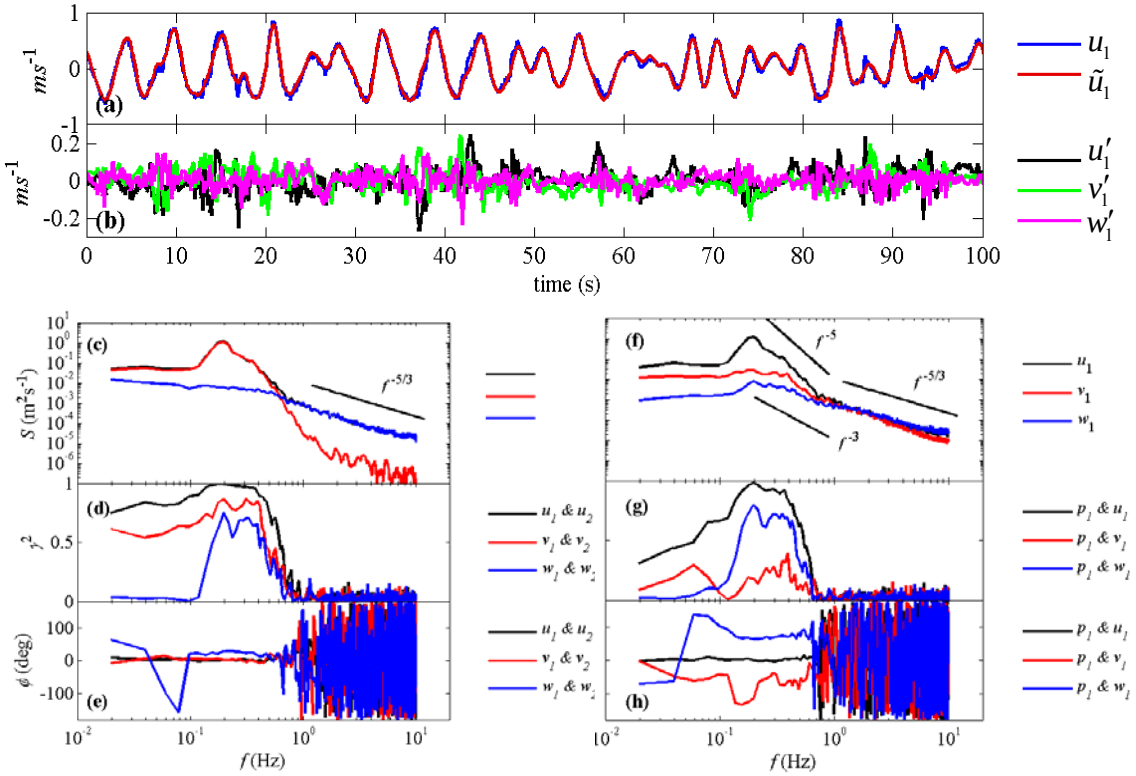

Figure 2. Example of turbulence decomposition, where S is the power spectral density, γ^2 is squared coherence, and ϕ is phase difference between the two analyzed quantities.

transformed into a coordinate system consisted of cross-shore (u), alongshore (v), and vertical velocities (w) based on the observed wave direction, where u denotes the cross-shore velocity in principle direction of wave orbital motion, v the orthogonal (alongshore) velocity of u in the horizontal plan.

The measured instantaneous velocity vector $\mathbf{u}$ over the reef can be decomposed into a mean component ($\overline{\mathbf{u}}$), a wave induced component ($\tilde{\mathbf{u}}$), and a turbulent component ($\mathbf{u}'$) as:

$$\mathbf{u} = \overline{\mathbf{u}} + \tilde{\mathbf{u}} + \mathbf{u}' , \tag{2}$$

where $\mathbf{u} = (u, v, w)$, $\overline{\mathbf{u}} = (\overline{u}, \overline{v}, \overline{w})$, $\tilde{\mathbf{u}} = (\tilde{u}, \tilde{v}, \tilde{w})$, and $\mathbf{u}' = (u', v', w')$. By taking time average over 20-minute duration of instantaneous velocity data, $\overline{\mathbf{u}}$ can be obtained. We used the differencing technique with adaptive least-square filter proposed by *Shaw and Trowbridge* (2001) to separate the wave and turbulent motions. This technique assumes the incoherent signals between the two ADVs to be turbulence, whereas the coherent signals to be wave motions; thus at least two vertically mounted ADVs are required for determining the turbulence. The wave induced velocity at position 1 is estimated from the filtered velocity, $\hat{U}_1$, being defined as

$$\hat{U}_1(t) = \int_{-T/2}^{T/2} \hat{h}(t-\tau) U_2(t) d\tau , \tag{3}$$

where T is a chosen filter length, $\hat{h}$ is the filter weights and U_2 is the velocity measured at position 2. The filter length T was chosen to be half of the peak wave period and a least square filter was used for $\hat{h}$:

$$\hat{\mathbf{h}} = \left(\mathbf{A}^{\mathrm{T}}\mathbf{A}\right)^{-1} \mathbf{A}^{\mathrm{T}}\mathbf{U}_1 . \tag{4}$$

Here $\mathbf{A}$ is an $M \times N$ windowed data matrix of velocity at position 2, where M is the number of data points and N is the number of filter weights; and $\mathbf{U}_1$ is the velocity vector at position 1. For the filtered estimates, all the three components of velocity measured at position 2 were used as inputs, resulting in $M \times 3N$ data matrix $\mathbf{A}$ with the number of degrees of freedom increasing by

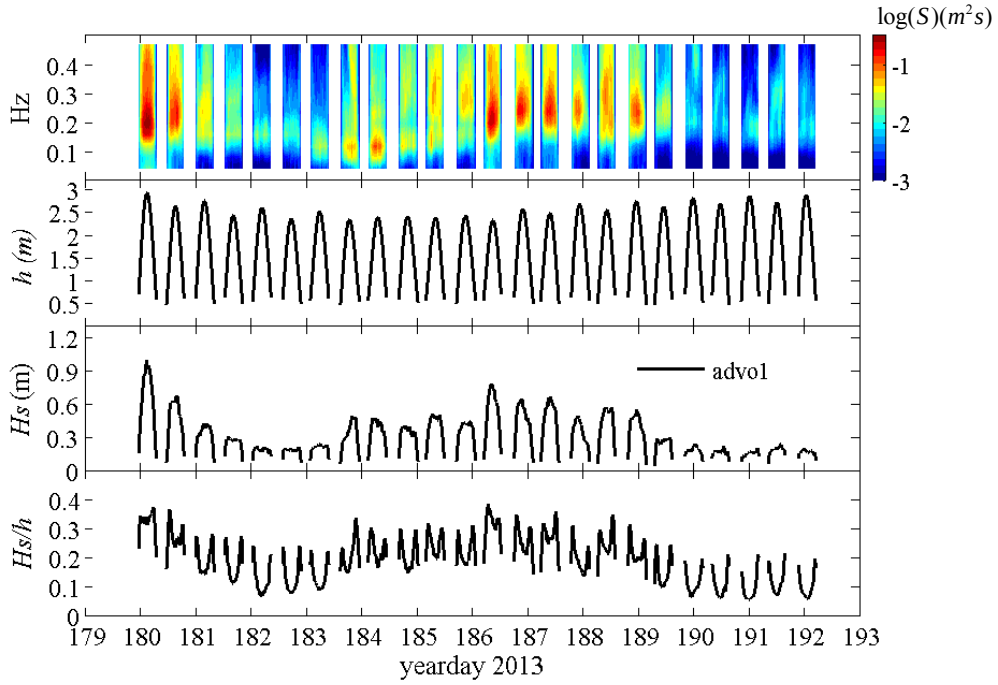

Figure 3. Time-series of wave and tide conditions. The top to bottom panels are the spectrogram of surface displacement at ADVO1, water depth (h) at advo1, significant wave height (H_s), and Ratio of H_s / h .

approximately a factor of 3. The coherent wave velocity vector at position 1, $\hat{U}_1$, is estimated by convolving the matrix $\mathbf{A}$ with $\hat{h}$:

$$\hat{\mathbf{U}}_1 = \mathbf{A}\hat{\mathbf{h}} . \tag{5}$$

The velocity vector of turbulent component at position 1 was estimated by

$$\Delta\hat{\mathbf{U}} = \mathbf{U} - \hat{\mathbf{U}}_1 \tag{6}$$

Figure 2a, b depict time series of the demeaned instantaneous velocity of 100 sec duration and its decomposed wave and turbulence components. The coherent motion at ADVO1 ($\tilde{\mathbf{u}}_1$, where subscript number denotes the number of ADVO) is estimated from the velocity data at ADVO2 using the ST01 method. The difference between the demeaned instantaneous velocity and the coherent wave motion results in turbulent velocity fluctuation ($\mathbf{u}_1'$). Figure 2c shows the spectra of the measured u_1 , v_1 , and w_1 . When performing the spectrum analysis, approximately 20-minute duration containing 28672 samples of velocity data were split into 27 segments using 50% overlap. Individual spectra of each segment were calculated using an FFT of 2048 samples with a Hanning window after mean removal and linear detrending. Spectra were then averaged to give 54 degrees of freedom. The energy spectra of the three components are approximately equal in the range from 0.9 to 4 Hz, which is higher than the surface-wave band; and exhibit the -5/3 slope characteristic of inertial subrange turbulence. In the frequency range of surface-wave band, the energy spectra of *u* and *v* are higher than that of *w*; both approximate the trend of f^3, which is similar to shallow water wave data in the surf zone (Thornton, 1979; Ruessink, 2010) and in a coral reef lagoon (Huang et al., 2012). For frequency higher than 4 Hz, the *v* component maintains the −5/3 power spectrum, whereas the spectra of *u* and *w* components exhibit lower powers; they are affected by the noise. Similar measurement noise levels in the higher frequency parts were also observed by *Ruessink* (2010) and *Huang et al.* (2012).

Figure 2f depicts velocity spectra of the demeaned u_1 , $\tilde{u}_1$ and u_1' . The spectrum of u approximately coincides with that of $\tilde{u}$ at low frequency range up to 0.7 Hz, indicating surface waves dominate the motion. For frequency higher than 0.8 Hz, the spectrum of u collapses with that of u', exhibits the −5/3 power in the range from 0.8 to 4 Hz, and flattens when f > 4Hz due to noise. Note that the component of u' also reveals the −5/3 power spectrum for frequency lower than 0.8 Hz. This suggests that the turbulence will be significantly underestimated if only the inertial subrange of u

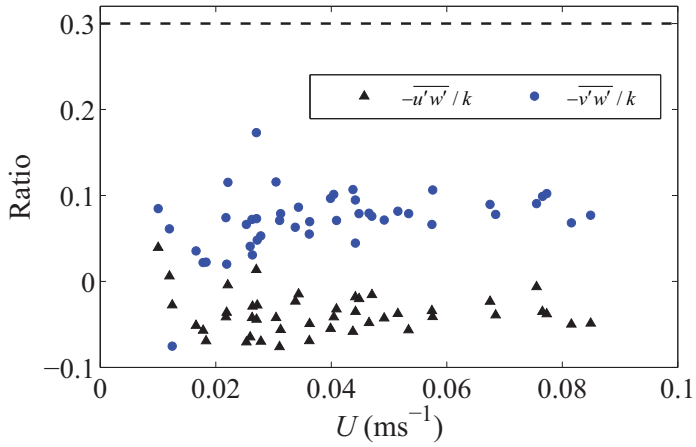

Figure 4. Ratios $-\overline{u'w'}/k$ and $-\overline{v'w'}/k$ versus current speed (U).

(typically distinguished by a high-pass filter) is considered to evaluate the fluctuations (Yoon and Cox, 2010).

The ST01 method assumes incoherent signals between the two ADVs are turbulence, whereas coherent signals are wave motion. Accordingly, it is useful to examine the squared coherence γ^2_{mn} and the phase difference ϕ_{mn}, where the subscripts denote the physical variables, between the two velocity series measured by the two ADVOs as shown in Figure 2g,h and between the velocity and pressure series as shown in Figure 2d,e. For the frequency range of surface waves from 0.1 to 0.7 Hz, all the squared coherence values, except that of γ^2_{pv}, are higher than 0.5. The values of γ^2_{uu} and γ^2_{pu} can reach higher than 0.95 near the peak frequency of surface waves (approximate from 0.14 to 0.24 Hz). Phase difference ϕ_{uu}, ϕ_{vv}, ϕ_{ww}, and ϕ_{pu} exhibit values close to zero, ϕ_{pw} approximates 90°, and ϕ_{pu} fluctuates in the frequency range of surface waves. This indicates a coherent wave motion in the cross-shore direction. High coherence values of γ^2_{uu} and γ^2_{ww} with zero phase difference in the frequency range of surface waves were also observed by Yoon and Cox (2010), but their observed value of γ^2_{vv} is very low due to the two-dimensional spectral waves in the flume.

Following Shaw and Trowbridge (2001) and Feddersen and Williams (2007), the quality of the estimated Reynolds stress, hence, of the decomposed velocity fluctuations, is accessed using the ogive curve testing (OgT) by examining the ogive curve of cospectra of $u'w'$ and $v'w'$. The nondimensional integrated cospectrum, i.e., the ogive for $\overline{v'w'}$, $Og_{v'w'}(f)$, is defined as follows (the same form for $\overline{u'w'}$):

$$Og_{v'w'}(f) = \frac{\int^{f} Co_{v'w'}(\hat{f})d\hat{f}}{u_*^2}, \tag{7}$$

where $Co_{v'w'}$ is the $\overline{v'w'}$ cospectrum. The ogive curve is expected to increase gently from 0 to 1 in the BBL of the atmosphere and in the ocean when there is minimum bias in the signals. Following Ruessink (2010), a narrower acceptance range of $Og_{v'w'}(f)$ is used in this study, i.e., $-0.3 < Og_{v'w'} < 1.3$. Hence, estimates of Reynolds stresses and other products of turbulent velocities when $Og_{v'w'}(f)$ is not in the range are marked. the possible wave bias contamination in estimated turbulence is also removed using the OgT.

3. RESULTS

3.1 Conditions of wind, waves, and tides

Time series of the wave and tidal conditions are presented in Figure 3. During the field experiment period, the significant wave height, Hs, ranges from 0 to 1 m, and local water depth, h,

ranges from 0 to 3 m. The ratio Hs/h ranges from 0.05 to 0.38 and most of the data are under nonbreaking waves. The wave induced velocity approximates 0 to 0.3 ms^{-1}, the current speed ranges between 0 to 0.1 ms^{-1}. The computed wave breaking index, *Hs/h,* ranges between 0.08- 0.35, and we used the criterion, i.e., *Hs/h* < 0.25 for identifying non-breaking waves conditions.

3.2 Ratios between turbulent shear stress and TKE

In the log-law region of current-alone BBL flows where the turbulence is in an equilibrium status, self-similarity of the turbulence statistics exists, and the Reynolds stress normalized by TKE, $-\overline{v'w'}/k$, approaches a constant value of 0.3 (Pope, 2000), where k is the TKE, as follows:

$$k = 0.5\left(\overline{u'^2} + \overline{v'^2} + \overline{w'^2}\right). \tag{8}$$

Turbulent shear stress (TSS) are normalized by the observed k and plotted against U as shown in Figure 4. Most $-\overline{u'w'}$ are negative because the vertical shear of the near-bed cross-shore flow changes its sign, which is consistent with the near-bed TSS estimates observed by Ruessink (2010). However, $-\overline{u'w'}$ becomes comparable to $-\overline{v'w'}$; this is possibly due to the wave-bias containment in TSS estimates. On the other hand, if the data failing the OgT have physical meanings, the data indicate that $-\overline{u'w'}$ is enhanced in low current speed possibly due to enhanced wave-current interaction because $-\overline{u'w'}$ is expected to be negligible in a current-alone BBL.

The observed mean value of $-\overline{v'w'}/k$ is consistently positive, at approximately 0.19 at the study site. This value is smaller than the canonical value of 0.3 in current-alone BBL flows (Pope, 2000), but larger than the value of 0.03~ 0.04 observed by Walter et al. (2011) in shallow tidal flow. This result indicates a lower shear production of $-\overline{v'w'}$, and suggests that the TKE may be also transported into the measurement volume. An examination of the transport mechanism is given in the following sections.

3.3 Terms in the TKE budget

The local change of the TKE is balanced by the following terms (Reynolds and Hussain, 1972)

$$\frac{\partial k}{\partial t} = P - \varepsilon + T_t + T_p + T_v + A_c + A_w + W_t, \tag{9}$$

where t is time, P is the shear production rate, ε is the turbulent dissipation rate, T_t is the vertical transport of TKE by turbulent fluctuations, T_p is the vertical transport of TKE due to fluctuating pressure, T_v is the viscous diffusion of TKE, A_c is the vertical advection transport of TKE by mean motion, A_w is the vertical advection transport of TKE by wave motion, and W_t is the transport of TKE energy between the turbulence and the wave motion. Because we can not measure the the dynamics pressure field using the preesented techniques, the transport from the fluctuating pressure, T_p, cannot be evaluated. The viscous diffusion, T_v, is negligible in the high Reynolds number flow of this study, and A_c is negligible because $\overline{w}$ is small in the BBL. In unstratified shallow coastal waters with horizontally homogenous turbulence statistics, the two terms associated with the waves, A_w and W_t, are evaluated as follows:

$$A_w = -\overline{\tilde{w}\frac{\partial k}{\partial z}}; \quad W_t = \overline{\left(-\langle u'w'\rangle\right)\frac{\partial \tilde{u}}{\partial z} + \left(-\langle v'w'\rangle\right)\frac{\partial \tilde{v}}{\partial z}}, \tag{10}$$

where the symbol $\langle\ \rangle$ denotes phase averaging as determined by the Hilbert transform. Comparing to the shear production and turbulent transport terms, the observed maximum magnitude of A_w and W_t are small and therefore negligible. The shear production rate of TKE by mean curernt, P, is computed as follows:

$$P = \frac{\boldsymbol{\tau}_t}{\rho} \cdot \left[\frac{\partial \overline{\mathbf{u}}}{\partial z} + \frac{\partial \mathbf{u}_s}{\partial z}\right] \tag{11}$$

We can only evaluted the vertical transport of TKE, T_t, which is defined as follows:

$$T_t = -\frac{\partial\left(\overline{k'w'}\right)}{\partial z}, \tag{12}$$

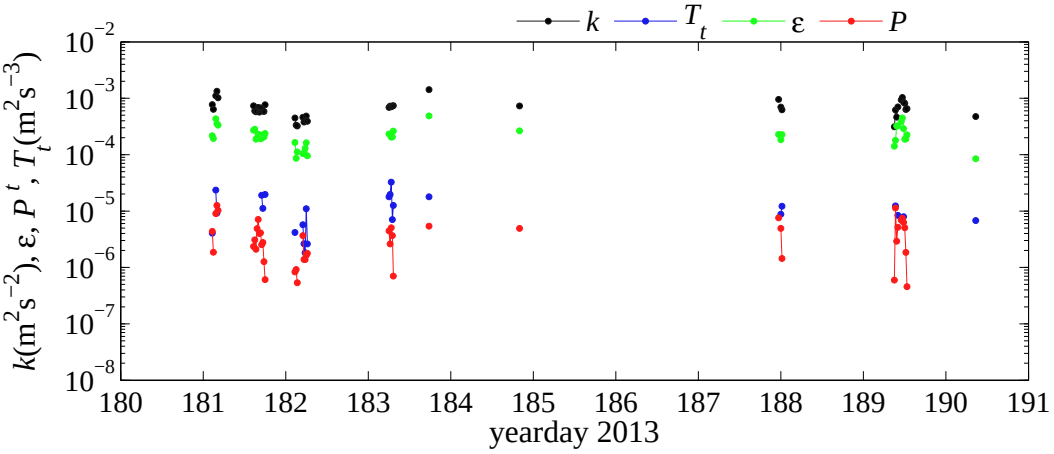

Figure 5. Time series of observed turbulent kinetic energy (k), vertical turbulent transport (T_t), turbulent dissipation rate (ε), and shear production by mean current (P).

where k' is the fluctuating TKE. Figure 5 shows time series of the observed TKE, ε, P, and T_t. Because the wave and current speeds are small during the experimental period, most of the estimated TSS did not pass the quality control of TSS. Although the good quality data are few, the results indeed show that T_t is comparable and sometimes larger than P. These two terms contribute to the source of ganing TKE, suggesting that transport term may be important for the dynamics in wave-current BBL. However, the two terms are smaller than the sink term, ε, suggesting that other tansport terms or other mechanisms should be importat, which might be amplified by the local inhomogeneous topograophy.

4. SUMMARY AND CONCLUSIONS

A twelve-day field observation of waves, current, and turbulence over a gravel beach was conducted using dual ADVO techniques. The measured instantaneous velocity field was analyzed to obtian the wave-induced and turbulent components using filtering techniques. The data quality of turbulence was controlled by removing wave biased data using ogive curve testing on TSS. The turbulent dissipation rate was estiamted using inertial subrange techniques. The ratio of the TSS to TKE is found to smaller than that in current-alone flow, suggesting that transport of TKE into the BBL might be important. The turublent dissipation rate is found to exceed the shear production, which also indicates the transport of TKE into the BBL might be important. After examining the most terms in the TKE budget as possiable, we found that the observed vertical turbulent transport is comparable to the shear production, and contributes to part of gaining TKE in the BBL. However, the available data is limited because the wave and current speed are small during the observational period. More qualified data and experiments on the gravel beach and a detailed comparisons of the result to different seabeds are needed to have a better understanding on the wave-current BBL over the naturally rough gravel beach.

ACKNOWLEDGMENTS

We thank the students in Graduate Institute of Hydrological and Oceanic Sciences, National Central University for their helps in field experiments. The Taiwan Socity of Ocean Engineering and the international wave dynamics research center, Ntioanal Cheng Kung University are acknowleded for their supports. This research was supported by grants from Ministry of Science and Technology, Taiwan, under contacts NSC 102-2611-M-008-004, MOST 103-2611-M-008-003 and NSC 101-2611-M-002-008-MY3.

REFERENCES

Conley, D.C. and Inman, D.L. 1992. Field observations of the fluid-granular boundary-layer under near-breaking waves, *Journal of Geophysical Research-Oceans*, 97(C6), 9631-9643.

Elgar, S., Raubenheimer, B. and Guza, R.T. 2005. Quality control of acoustic Doppler velocimeter data in the surf zone, *Measurement Science & Technology*, 16, 1889-1893.

Feddersen, F. 2012. Observations of the Surf-Zone Turbulent Dissipation Rate, *Journal of Physical Oceanography*, 42(3), 386-399.

Feddersen, F., Trowbridge, J.H. and Williams, A.J. 2007. Vertical structure of dissipation in the nearshore, *Journal of Physical Oceanography*, 37, 1764-1777.

Feddersen, F. and Williams, A.J. 2007. Direct estimation of the Reynolds stress vertical structure in the nearshore, *Journal of Atmospheric and Oceanic Technology*, 24(1), 102-116.

Foster, D.L., Beach, R.A. and Holman, R.A. 2000. Field observations of the wave bottom boundary layer, *Journal of Geophysical Research-Oceans*, 105(C8), 19631-19647.

Foster, D.L., Beach, R.A. and Holman, R.A. 2006. Turbulence observations of the nearshore wave bottom boundary layer, *Journal of Geophysical Research-Oceans*, 111(C4), C04011.

Grant, W.D. and Madsen, O.S. 1979. Combined wave and current interaction with a rough bottom, *Journal of Geophysical Research-Oceans*, 84(C4), 1979-1808.

Grant, W.D. and Madsen, O.S. 1986. The continental-shelf bottom boundary layer, *Annual Review of Fluid Mechanics*, 18, 265-305.

Grasso, F., Castelle, B. and Ruessink, B.G. 2012. Turbulence dissipation under breaking waves and bores in a natural surf zone, *Continental Shelf Research*, 43, 133-141.

Gross, T.F. and Nowell, A.R. 1983. Mean flow and turbulence scaling in a tidal boundary layer, *Continental Shelf Research*, 2, 109-126.

Huang, Z.C. et al. 2012. Dissipation of wave energy and turbulence in a barrier-reef lagoon, *Journal of Geophysical Research-Oceans*, 117, C03015.

Jones, N.L. and Monismith, S.G. 2008. The influence of whitecapping waves on the vertical structure of turbulence in a shallow estuarine embayment, *Journal of Physical Oceanography*, 38(7), 1563-1580.

Mori, N., Suzuki, T. and Kakuno, S. 2007. Noise of acoustic Doppler velocimeter data in bubbly flows, *Journal of Engineering Mechanics-ASCE*, 133(1), 122-125.

Perlin, A. et al. 2005. A modified law-of-the-wall applied to oceanic bottom boundary layers, *Journal of Geophysical Research-Oceans*, 110(C10), C10s10.

Pope, S.B. 2000. *Turbulent flows*. Cambridge Univ. Press, New York.

Reidenbach, M.A., Monismith, S.G., Koseff, J.R., Yahel, G. and Genin, A. 2006. Boundary layer turbulence and flow structure over a fringing coral reef, *Limnology and Oceanography*, 51(5), 1956-1968.

Reynolds, W.C. and Hussain, A.K.M.F. 1972. The mechanics of an organized wave in turbulent shear flow. Part 3. Theoretical models and comparisons with experiments, *Journal of Fluid Mechanics*, 54, 263-288.

Ruessink, B.G. 2010. Observations of Turbulence within a Natural Surf Zone, *Journal of Physical Oceanography*, 40(12), 2696-2712.

Sanford, T.B. and Lien, R.C. 1999. Turbulent properties in a homogeneous tidal bottom boundary layer, *Journal of Geophysical Research-Oceans*, 104(C1), 1245-1257.

Shaw, W.J. and Trowbridge, J.H. 2001. The direct estimation of near-bottom turbulent fluxes in the presence of energetic wave motions, *Journal of Atmospheric and Oceanic Technology*, 18(9), 1540-1557.

Smyth, C. and Hay, A.E. 2003. Near-bed turbulence and bottom friction during SandyDuck97, *Journal of Geophysical Research-Oceans*, 108, C63197.

Thompson, C.E.L., Williams, J.J., Metje, N., Coates, L.E. and Pacheco, A. 2012. Turbulence based measurements of wave friction factors under irregular waves on a gravel bed, *Coastal Engineering*, 63, 39-47.

Thornton, E.B. 1979. Energetics of breaking waves within the surf zone, *Journal of Geophysical Research-Oceans and Atmospheres*, 84(NC8), 4931-4938.

Trowbridge, J.H. and Agrawal, Y.C. 1995. Glimpses of a wave boundary-layer, *Journal of Geophysical Research-Oceans*, 100(C10), 20729-20743.

Walter, R.K., Nidzieko, N.J. and Monismith, S.G. 2011. Similarity scaling of turbulence spectra and cospectra in a shallow tidal flow, *Journal of Geophysical Research-Oceans*, 116, C10019.

Yoon, H.D. and Cox, D.T. 2010. Large-scale laboratory observations of wave breaking turbulence over an evolving beach, *Journal of Geophysical Research-Oceans*, 115, C10007.